Chemical Engineering Journal 411 (2021) 128506

Contents lists available at ScienceDirect

Chemical Engineering Journal

journal homepage: www.elsevier.com/locate/cej

Hydrogen-bonded network enables semi-interpenetrating ionic conductive hydrogels with high stretchability and excellent fatigue resistance for capacitive/resistive bimodal sensors

Ao Wang [a], Yufeng Wang [a], Bing Zhang [a], Kening Wan [c], Jixin Zhu [d], Jingsan Xu [e], Chao Zhang [a,*], Tianxi Liu [a,b,*]

[a] State Key Laboratory for Modification of Chemical Fibers and Polymer Materials, College of Materials Science and Engineering, Key Laboratory of High Performance Fibers & Products, Ministry of Education, Innovation Center for Textile Science and Technology, Donghua University, Shanghai 201620, China
[b] Key Laboratory of Synthetic and Biological Colloids, Ministry of Education, School of Chemical and Material Engineering, Jiangnan University, Wuxi 214122, China
[c] School of Engineering and Materials Science, Queen Mary University of London, Mile End Road, London E1 4NS, UK
[d] Shaanxi Institute of Flexible Electronics (SIFE), Northwestern Polytechnical University (NPU), 127 West Youyi Road, Xi'an 710072, China
[e] School of Chemistry, Physics and Mechanical Engineering, Queensland University of Technology, Brisbane, QLD 4001, Australia

ARTICLE INFO

Keywords:
Ionic conductive hydrogels
Hydrogel-network constrained polymerization
Hydrogen-bonded network
Stretchability
Wearable ionic sensor

ABSTRACT

The construction of ionic conductive hydrogels with complex deformation tolerance and excellent fatigue resistance is highly demanded yet challenging. Herein, a semi-interpenetrating ionic conductive hydrogel (SICH) is fabricated by a hydrogel-network constrained polymerization of 1-butyl-3-vinylimidazole tetrafluoroborate and acrylic acid in polyethylene oxide aqueous solution. Ascribing to the formation of a dense intermolecular hydrogen-bonded network, the SICH is capable of being stretched up to ~300%, compressed to ~85%, and recovered immediately when the external force is fully released. The SICH can readily work as a high deformation-tolerant ionic conductor for capacitive/resistive bimodal ionic sensors. The ionic sensor not only showed a wide response range to dynamic pressures (0–8 kPa) and excellent cycling stability (500 cycles) in a capacitive mode, but also demonstrated high sensitivity (gauge factor of ~1.1), excellent linear response (0–300% strain) and fast response time (80 ms) in a resistive mode. As a demonstration, a wearable bimodal SICH ionic sensor was assembled, showing high sensitivity, linearity, wide response range and great durability in detecting complex human motions including speaking and various joint bending.

1. Introduction

Skin-inspired sensors that imitate functions of human skin by converting external stimuli into easily processed electric signals show broad applications in health monitoring,[1–3] soft robotics,[4,5] and human–machine interactions.[6,7] By replacing conventional electric conductors with emerging ionic conductors, ionic sensors are capable of monitoring external stimuli rapidly and in real-time through the capacitive and resistive sensing mechanism.[8–13] The capacitive ionic sensors present the advantages of low hysteresis, excellent sensitivity and high stability.[14–16] But they exist a narrow response range and easily-interrupted signals due to insufficient mechanical strength and low deformation-tolerant performance of typically ionic conductors of hydrogels and ionogels.[17,18] Conversely, the resistive ionic sensors are anti-interference while exhibiting a non-linear response and poor cycling stability.[19–21] Therefore, the development of an ionic sensor that works in a bimodal capacitive/resistive mode is promising, because it is expected to demonstrate an integrated performance of high deformation tolerance and linear sensitivity in a wide response range. However, challenges were confronted to achieve this due to the lack of high fatigue-resistant ionic conductors with large linearity and high sensitivity in a wide deformation range.[22,23]

Poly(ionic liquid) (PIL) hydrogel is a three-dimensional hydrogel network that is polymerized from charged ionic liquid monomers in substantial water. It usually has great biocompatibility and comparably mechanical flexibility to human skin and is expected to demonstrate

* Corresponding authors at: State Key Laboratory for Modification of Chemical Fibers and Polymer Materials, College of Materials Science and Engineering, Key Laboratory of High Performance Fibers & Products, Ministry of Education, Innovation Center for Textile Science and Technology, Donghua University, Shanghai 201620, China.
E-mail addresses: czhang@dhu.edu.cn (C. Zhang), txliu@fudan.edu.cn (T. Liu).

https://doi.org/10.1016/j.cej.2021.128506
Received 6 November 2020; Received in revised form 22 December 2020; Accepted 11 January 2021
Available online 17 January 2021
1385-8947/

high elasticity and moderate ionic conductivity for ionic sensors. [2,9,24–26] However, the development of PIL hydrogels with high mechanical robustness, complex deformation-tolerant performance and excellent fatigue resistance is essential but challenging. Fortunately, the chemical crosslinking and physical interactions are two common strategies to enhance the mechanical strength and fatigue resilience of PIL hydrogels.[27–31] The chemical crosslinking can notably enhance the mechanical strength of PIL hydrogels,[32,33] but the fracture of these covalent chemical bonds under large deformation gives rise to irreversible damages to the structure, resulting in poor deformation-tolerant and fatigue-resistant performance. On the contrary, physical interactions can endow PIL hydrogels with highly deformation-tolerant and excellent fatigue-resistant performance due to the easy recovery and rebuilding of the physical network under deformation.[34–36] However, their low bond energy and crosslinking density usually lead to the mechanical strength of hydrogels failing to meet the actual demands for ionic sensors.

Herein, a semi-interpenetrating ionic conductive hydrogel (SICH) was fabricated by a hydrogel-network constrained polymerization of 1-butyl-3-vinylimidazole tetrafluoroborate (BVIT) and acrylic acid (AA) in polyethylene oxide (PEO) aqueous solution. The semi-interpenetrating network is composed of a covalently cross-linked network of poly (acrylic acid)-random-poly(1-butyl-3-vinylimidazole tetrafluoroborate) (PAA-r-BVIT) and an interspersed network of PEO. The as-obtained SICH showed superelasticity with large reversible stretchability/compressibility and excellent fatigue resistance ascribing to the formation of a dense hydrogen-bonded network between the PAA-r-BVIT and PEO chains. The SICH can readily serve as a highly deformation-tolerant ionic conductor for capacitive/resistive bimodal ionic sensors. The bimodal ionic sensor operated in the capacitive mode demonstrated a wide pressure response range and high fatigue resistance in 500 loading/unloading cycles. In the resistive mode, the ionic sensor exhibited a high sensitivity with a gauge factor of 1.1, linearity over a tensile strain range of 0–300% and fast response time within 80 ms. As a proof of concept, a wearable bimodal SICH sensor was assembled, achieving real-time monitoring of complex human motions of speaking, finger bending, elbow bending and knee bending. This study provides a new path of developing ionic conductive hydrogels with high mechanical elasticity and fatigue resilience for ionic sensors with linearity, high sensitivity and durability.

2. Materials and methods

2.1. Chemicals and reagents

PEO (average $Mv = 600000$), AA (AR, >99%, distilled before use), ammonium persulfate (APS, AR, ≥98%), *N*,*N*'-methylene-bis(acrylamide) (MBAA, 96%) were purchased from Aladdin Chemicals. 1-butyl-3-vinylimidazole-based ionic liquids with various counter anions (Cl^-, I^-, NO_3^-, BF_4^-) were purchased from Shanghai Chengjie Chemicals. Deionized water was used throughout the experiment. All the chemicals were used as received unless otherwise stated.

2.2. Preparations of hydrogel samples of SICH, PAA-r-BVIT and PAA/PEO

The aqueous solution of 10 wt% AA, 3 wt% PEO, APS (1 mol% of monomers), MBAA (0.5 mol% of monomers) and designed amounts of BVAT was mixed, poured into a polytetrafluoroethylene (PTFE) mold, polymerized at 60 °C for 12 h in a nitrogen atmosphere. The SICH-1, SICH-2, SICH-3 and SICH-4 represent as-prepared hydrogel samples with an AA/BVIT molar ratio of 1/1, 3/1, 5/1, and 7/1, respectively. For comparison, a hydrogel sample of PAA-r-BVIT was prepared following the above steps, but without the addition of PEO. A hydrogel sample of PAA/PEO was prepared as described above without the addition of BVIT.

2.3. Measurements of bimodal ionic sensors

The bimodal ionic sensor was assembled by using two as-prepared hydrogel samples (10 × 5 × 2 mm^3) and a 3 M VHB 4905 film (thickness: 0.5 mm) as the electrode and dielectric layer, respectively. The capacitance of the bimodal ionic sensor was calculated by the following equation:

$$C = \frac{\varepsilon A}{4\pi k d} \tag{1}$$

where C is the capacitance, ε is the dielectric constant of dielectric layer, k is the electrostatic constant, A is the effective area of hydrogel samples, and d is the thickness of dielectric layer.

The capacitive sensing performance was measured by an LCR Meter (TH 2832). The capacitive response, sensitivity (S_c) and gauge factor (GF_c) were calculated by the following equations:

$$\frac{\Delta C}{C_0} = \frac{C - C_0}{C_0} \tag{2}$$

where C_0 is the initial capacitance, and C is the real-time capacitance under deformation.

$$S_c = \frac{\Delta C / C_0}{P} \tag{3}$$

where P is the applied pressure.

$$GF_c = \frac{\Delta C / C_0}{\varepsilon} \tag{4}$$

where ε is the applied strain.

The resistive sensing performance of the bimodal ionic sensor was measured by a Keithley 2400 digital source meter. Two Cu foils were sandwiched with one piece of hydrogel samples in the as-assembled bimodal ionic sensor. The relative resistance variation ($\Delta R/R$), sensitivity (S_r) and gauge factor (GF_r) of the resistive sensor were calculated by the following equations:

$$\frac{\Delta R}{R_0} = \frac{R - R_0}{R_0} \tag{5}$$

where R_0 is the initial resistance, R is the real-time resistance under deformation.

$$S_r = \frac{\Delta R / R_0}{P} \tag{6}$$

where P is the applied pressure.

$$GF_r = \frac{\Delta R / R_0}{\varepsilon} \tag{7}$$

where ε is the applied strain.

3. Results and discussion

A schematic representation of the preparation procedure of the SICH is illustrated in Fig. 1a. The SICH with a semi-interpenetrating network was in-situ formed by hydrogel-network constrained polymerization of BVIT and AA monomers in PEO aqueous solution. A physical and chemical dual-crosslinking was simultaneously achieved during the space-constrained polymerization, i.e., a chemically cross-linked random copolymer (PAA-r-BVIT) with an intramolecular electrostatic interaction was in-situ formed, whereas an intermolecular hydrogen-bonded interaction between the PEO and PAA-r-BVIT was simultaneously achieved. During the hydrogel-network constrained polymerization, the reaction solution of SICH and PAA/PEO (comparison sample of in-situ polymerized AA in PEO aqueous solution) changed from transparent to milky white within 0.5 h (Fig. 1b), indicating the

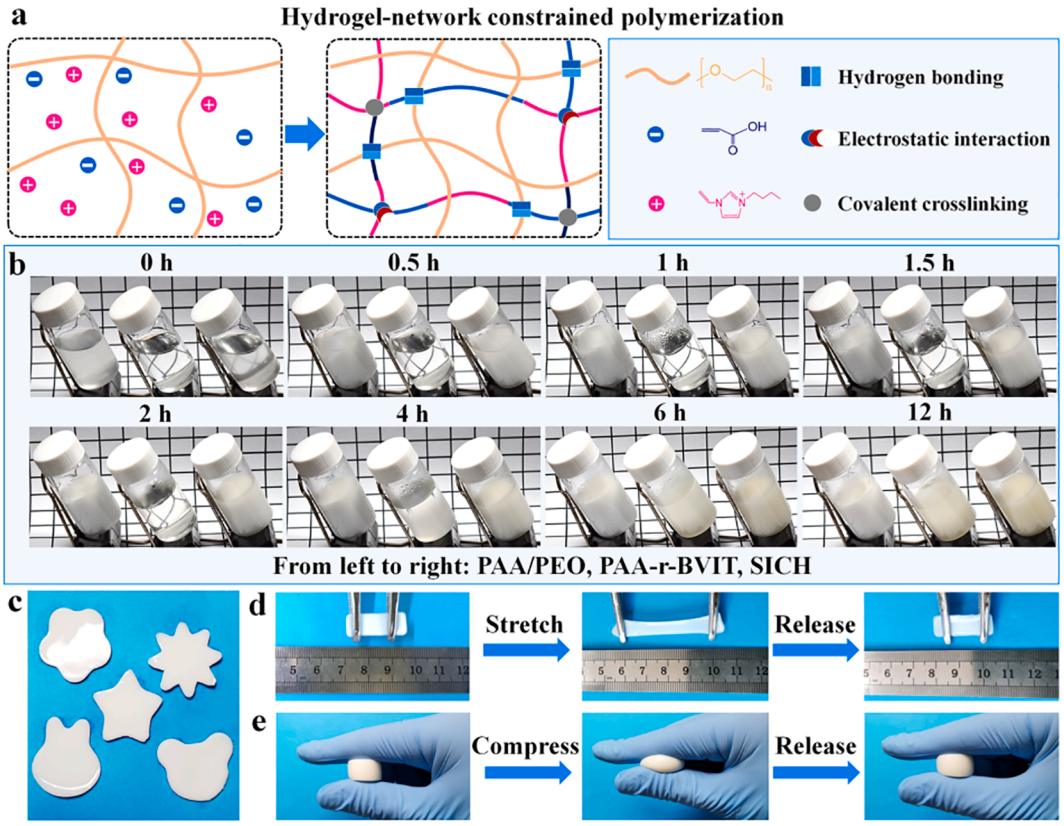

Fig. 1. (a) Schematic of the preparation procedure of the SICH by the hydrogel-network constrained polymerization. (b) Photographs showing in-situ polymerization processes. From left to right: PAA/PEO, PAA-r-BVIT and SICH. (c) Photograph showing the SICH in various shapes. Photographs showing the SICH during (d) stretching-releasing and (e) compressing-releasing processes, respectively.

formation of a dense hydrogen-boned network ascribing to interactions between the PEO and initially polymerized PAA segments. The polymerization rates of AA and BVIT in an aqueous solution were investigated. ^{1}H NMR spectra of a comparison sample of neat PAA showed peaks at 1.6–1.8 ppm ascribed to H-b and H-c, and 2.4 ppm ascribed to H-a (Fig. S1a). The results showed that the polymerization rate of AA in water was fast, and most of the monomers were consumed within 60 min after polymerization. However, peaks corresponding to the PBVIT in the control sample were not obvious even after polymerizing for 60 min (Fig. S1b). The hydrogen-bonded interaction between AA monomers and water might accelerate their reactivity ratios during the copolymerization.[37] The AA monomers exhibited a much faster polymerization rate than that of BVIT, further proving that the subsequent copolymerization of AA and BVIT was space-constrained within the initially polymerized hydrogel network of PAA/PEO. It is worth mentioning that the SICH is capable of being shaped and cut into various shapes by changing reaction vessels and tailoring (Fig. 1c). The resultant SICH is capable of being stretched up to ~300%, compressed to ~85%, and recovered immediately upon the external force released (Fig. 1d, 1e, Movies S1, S2), demonstrating highly stretchable and compressible performance along with excellent reversibility.

The in-situ polymerizations of ionic liquid monomers of 1-butyl-3-vinylimidazole with a variety of counter anions were investigated. The BVIT is a commonly used monomer of PIL with unique properties of low saturated vapor pressure, high thermal stability and high ionic conductivity.[38,39] Types and sizes of counter anions might greatly affect the water solubility, ionic conductivity and aggregation state of ionic liquid monomers.[40–42] Ionic liquid monomers containing different counter anions of ions Cl^-, I^-, NO_3^- and BF_4^- were compared (Fig. S2a). Polymerizations of 1-butyl-3-vinylimidazole monomers containing Cl^- and NO_3^- anions in water were relatively difficult and the viscosity of the reaction system is too low to sustain a certain shape even after 24 h (Fig. S2b). Chemical reduction reactions between the I^- anions and initiators easily occurred accompanied with the formation of I_2 (Fig. S2b). Besides, no commercial 1-butyl-3-vinylimidazole monomers containing the SO_4^{2-} anions were obtained. Considering the matching principle of polymerization rate with AA for the co-polymerization and the cost, the 1-butyl-3-vinylimidazole monomer with BF_4^- anions was used in this study. Fig. S3 further showed fracture-surface SEM images of freeze-dried hydrogel samples of SICH, PAA/PEO and PAA-r-BVIT. Due to the presence of highly charged chains, the PAA-r-BVIT exhibited a dense lamellar structure, while the PAA/PEO exhibited a uniform pore size distribution. From SEM images of SICH-3, relatively ordered pore distribution and relatively compact network structure were observed, which was conducive to the excellent mechanical properties.

The intermolecular hydrogen-bonded interaction among the SICH was verified by Fourier Transform Infrared (FTIR) spectra (Fig. 2a). The characteristic peak at ~1553 cm^{-1} corresponding to the stretching vibration of the imidazole ring skeleton indicated that ionic conductive BVIT segments were introduced into the SICH.[43] A new and wide absorption peak appeared at 3200–3600 cm^{-1} when the PEO was introduced, indicating that an intermolecular hydrogen-bonded was formed between the PAA segments and PEO chains. The stretching vibration of C=O on carboxyl groups shifted from 1705 cm^{-1} of neat PAA to 1713 cm^{-1} of PAA/PEO (Fig. 2b). The stretching vibration peak at 1045 cm^{-1} ascribed to the B-F bond among the PAA-r-BVIT shifted to 1054 cm^{-1} of the SICH-1 (Fig. 2c). The absorption peaks of C=O and B-F moving towards high wavenumbers indicated that the formation of the intermolecular hydrogen bonds.[43,44] Besides, the absorption peak near 1570 cm^{-1} caused by the stretching asymmetric vibration of carboxyl acid groups demonstrated the existence of intramolecular electrostatic interactions in the PAA-r-BVIT and SICH.[45–47]

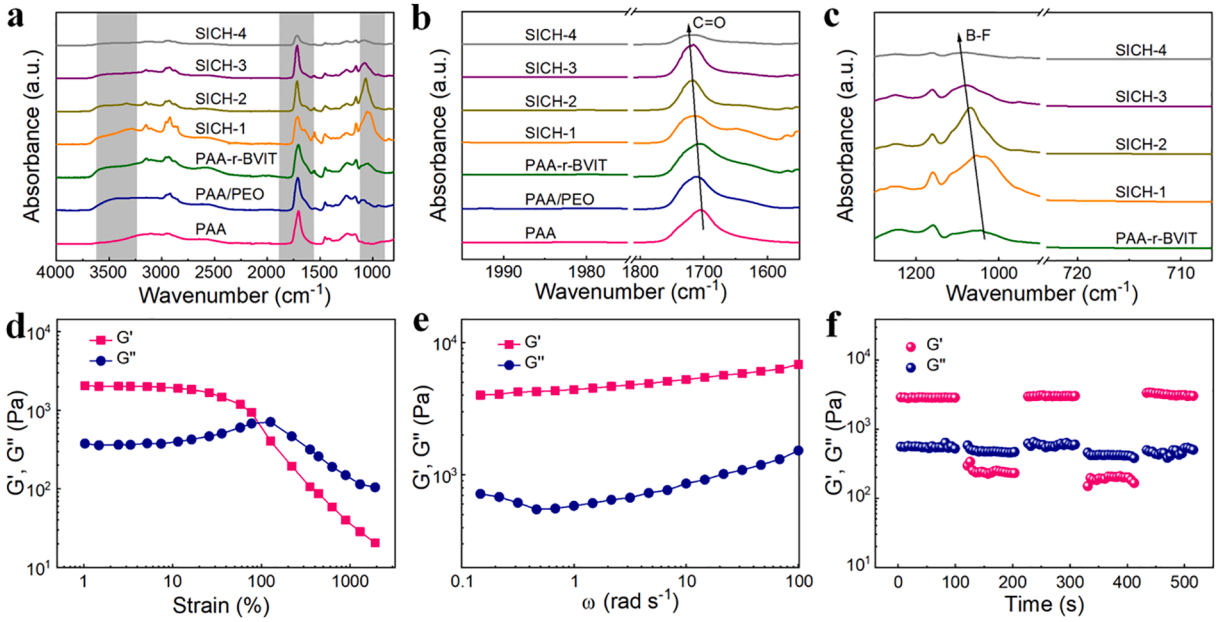

Fig. 2. (a) Full-range and (b) enlarged FTIR spectra of freeze-dried hydrogel samples of SICH, PAA-r-BVIT, PAA/PEO and PAA. (c) Enlarged FTIR spectra of freeze-dried hydrogel samples of SICH and PAA-r-BVIT. (d) Oscillatory amplitude sweep test (strain: 1%–1000%) at an angular frequency of 5 rad s^{-1} for the SICH-3. (e) Oscillation frequency sweep test at a shear strain of 0.1% for the SICH-3. (f) Alternate step strain sweep test with alternating shear strains of 1% and 500% with 100 s at a constant angular frequency of 5 rad s^{-1} for the SICH-3.

Dynamic rheological tests were performed to investigate the viscoelastic properties of SICH. An oscillatory amplitude sweep test was conducted to determine the linear viscoelastic region of SICH-3 (Fig. 2d). The storage moduli (G') of SICH always exceeded its loss moduli (G'') under a small shear strain (<100%), due to neglected deformation damages of hydrogel structures, revealing excellent structural integrity of SICH. When the hydrogel underwent a large shear strain, the G' of SICH began to gradually decline and its G'' value became higher than that of G'. This is because the physical bonds within the hydrogel were dissipated, and the solid-like elastic network structure of the hydrogel was destroyed and translated into viscous fluids.[48] An oscillation frequency sweep test was conducted under a small shear strain to observe the frequency dependence of the viscoelastic properties of SICH-3 (Fig. 2e). The G' and G'' exhibited an intense dependence on the angular frequency, and the G' always exceeded the G'' over the entire angular frequency sweep range, revealing an elastic nature of hydrogels.[48–50] Structural damages along with the transformation of G' and G'' values were observed among hydrogel samples of PAA-r-BVIT and PAA/PEO (Fig. S4a), indicating their poor ability to maintain structural integrity under large deformation. Fig. S4b indicated the elastic state of hydrogel samples of PAA-r-BVIT and PAA/PEO. The G' and G'' values of PAA-r-BVIT failed to return to the original value after undergoing a large shear strain of 200% (Fig. S4c), indicating its poor recovery ability. On the contrary, the G' and G'' values of PAA/PEO were almost restored even though it experienced a large shear strain of 200% (Fig. S4d). The deformation recovery performance of SICH-3 was also evaluated by the alternating step strain sweep test (Fig. 2f). A small shear strain of 1% and large shear strain of 500% were applied to SICH-3, respectively, and maintained for 100 s at each step. Originally, the G' kept at 2900 Pa and was higher than G'' under a small shear strain of 1%, indicating that the hydrogels maintained the stability of a solid-like elastic network under a small shear strain. When hydrogels experienced a large shear strain of 500% subsequently, the G' dropped down to 230 Pa and was inferior to the corresponding G''. At this point, the elastic network structure of SICH was destroyed, showing a liquid-like viscous behavior. Surprisingly, when the shear strain returned to 1%, the G' immediately exceeded the G'' and almost maintained a similar value as it was in the initial state. This reveals a rapid recovery ability of the SICH.

Mechanical properties of SICH samples were measured to explore the effect of the semi-interpenetrating network on their mechanical properties. The tensile mechanical properties of SICH samples with tailored AA/BVIT ratios were investigated (Fig. 3a). Except for the hydrogel sample of PAA-r-BVIT with large brittleness, other hydrogel samples can be stretched for the tensile tests. The fracture strength and Young's modulus of hydrogel samples of SICH-1, SICH-2, SICH-3, SICH-4 and PAA/PEO were summarized in Table S1. The SICH samples with a semi-interpenetrating network exhibited largely enhanced mechanical properties compared to hydrogel samples of PAA/PEO and PAA-r-BVIT. Besides, the mechanical strength and Young's modulus of SICH samples were significantly improved when the BVIT content among the SICH increased. Successive loading–unloading tensile tests were conducted under tensile strains of 50%, 100%, 150%, 200% (Fig. 3b), respectively. No residual strain appeared when the successive tensile strain increased from 50% to 200%. The loading curves almost overlapped with the unloading curves under the various tensile strains. The small hysteresis loops demonstrated a highly deformation-tolerant performance of SICH-3, related to the high density of the intermolecular hydrogen bonds. Subsequently, the loading–unloading tensile tests under the tensile strain of 200% were performed to investigate the fatigue resistance of SICH-3 (Fig. 3c). A large hysteresis loop appeared in the first cycle due to fractures of covalent bonds and reversible interactions. Nevertheless, subsequent cycles exhibited smaller hysteresis loops as a consequence of permanent damages of covalent bonds and the fast recovery of reversible hydrogen bonds. Further, the fatigue resistance characteristics of SICH-3 were quantitatively analyzed by the loss of maximum stress (strength) and Young's modulus (stiffness) under different cycles (Fig. S5a). Except that the maximum stress and Young's modulus dropped greatly in the first 50 cycles, they kept constant basically in other cycles. The energy loss coefficient was ~0.2 (Fig. S5b), demonstrating its good elastic property.

Compressive mechanical tests were performed to further evaluate the mechanical properties of SICH. Among them, the hydrogel sample of PAA-r-BVIT exhibited a stiff and brittle network while the hydrogel sample of PAA/PEO showed a soft and weak network (Fig. 3d). Conversely, the SICH samples could not only withstand a large compressive strain of 85% but also had a highly deformation-tolerant

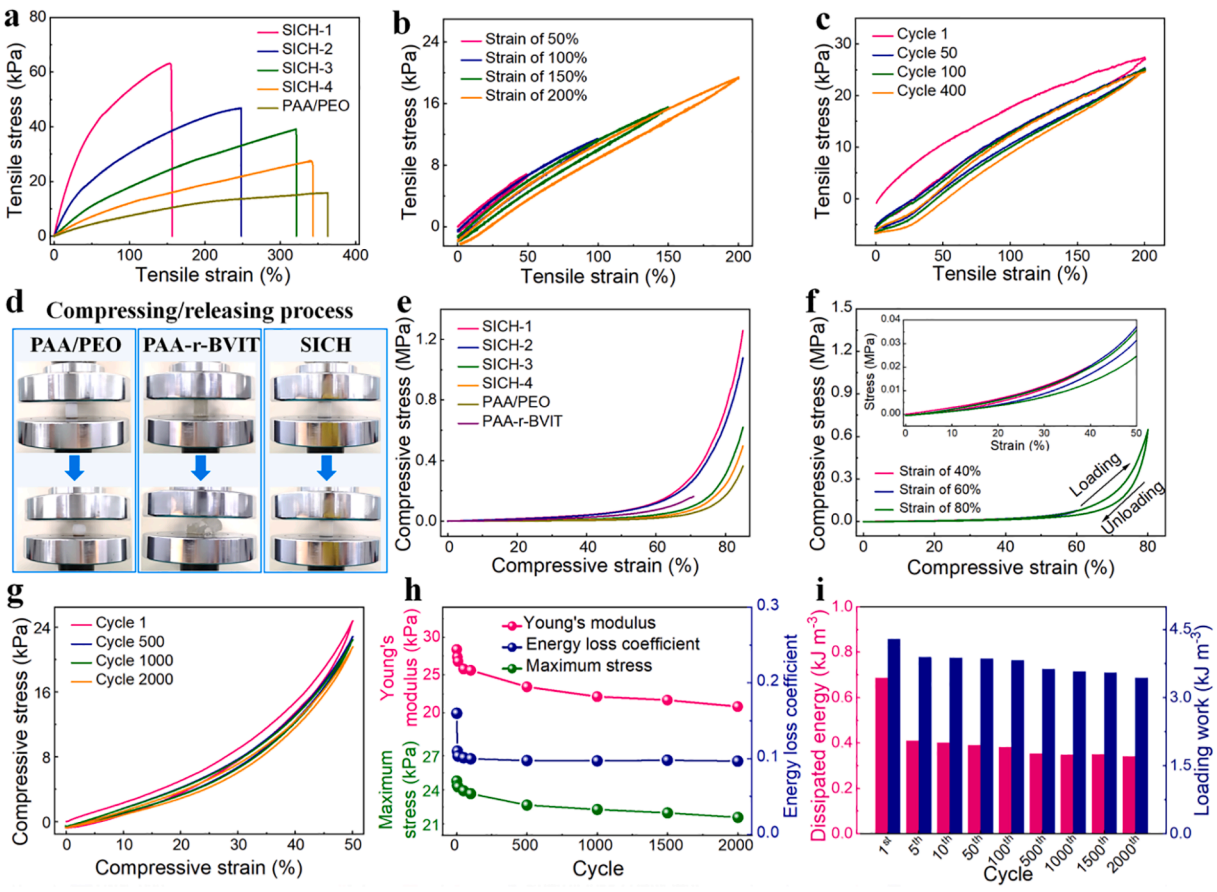

Fig. 3. Mechanical properties of SICH. (a) Tensile stress–strain curves of the PAA/PEO and SICH hydrogels. (b) Stress–strain curves of the SICH-3 at various tensile strains. (c) Tensile fatigue test of SICH-3 at a strain of 200%. (d) Photographs showing the reversible compression behaviors of PAA/PEO, PAA-r-BVIT and SICH hydrogels. (e) Compressive stress–strain curves of PAA/PEO, PAA-r-BVIT and SICH hydrogels. (f) Stress–strain curves of SICH-3 at various compressive strains. (g) Compressive fatigue test of SICH-3 at a strain of 50%. History of (h) Young's modulus, energy loss coefficient, maximum stress and (i) dissipated energy and loading work of the SICH-3 as a function of the compressive cycles.

performance. The highly deformation-tolerant performance of these SICH samples was closely related to the high-density intermolecular hydrogen-bonded network and covalent-bonded network, providing an excellent elastic network by preventing hydrogels from severe damages. Fig. 3e indicates the hydrogel sample of PAA-r-BVIT only withstands a compressive strain of 70% with a modulus of 22.7 kPa and exhibits a large brittleness, which is related to its high covalent cross-linking density. The hydrogel sample of PAA/PEO with a modulus and strength of 0.37 MPa and 6.3 kPa, respectively, exhibited poor mechanical properties (Table S2), ascribed to its low hydrogen-bonded density. Besides, the compressive strength and modulus of SICH samples gradually decreased with an increased AA/BVIT ratio. For instance, the SICH-1 exhibited high mechanical strength and modulus of 1.26 MPa and 72.2 kPa, respectively, while the SICH-4 only had a mechanical strength and modulus of 0.5 MPa and 10.1 kPa, respectively. This is attributed to the weakened intramolecular electrostatic interactions and intensified intermolecular hydrogen-bonded interactions in the semi-interpenetrating network.[51] Furthermore, the SICH-3 immediately recovered to its original state through the successive compressive strains (40%, 60% and 80%) without intermittences (Fig. 3f), demonstrating the highly deformation-tolerant performance. A cyclic compressive fatigue resistance performance of the SICH-3 was measured for 2000 cycles under a compressive strain of 50% (Fig. 3g). A large hysteresis loop appeared in the first cycle due to fractures of covalent bonds and reversible interactions. Subsequent cycles exhibited smaller hysteresis loops as a consequence of permanent damages of covalent bonds and the fast recovery of the reversible intermolecular hydrogen-bonded network. The almost identical hysteresis loops after 2000 compression cycles indicated that the SICH-3 showed a highly deformation-tolerant performance and excellent fatigue resistance. Further, the compressive fatigue resistance characteristics of the SICH-3 were quantitatively analyzed by the loss of maximum stress (strength) and Young's modulus (stiffness) under different cycles (Fig. 3h). Their maximum stress and Young's modulus greatly decreased in the first 50 cycles, and afterward, they decreased slightly and tended to stabilize, remaining above 74% after the 2000 cyclic test. The energy loss coefficient, i.e., the ratio of dissipated energy to loading work (Fig. 3i), was small, indicating a little damage to the hydrogel network with an elastomer-like property. [52,53] Except for the first cycle, where the energy loss coefficient was 0.16, it stabilized at 0.097 in the following cycles (Fig. 3h). This value was smaller than other SICH samples, indicating the highest deformation-tolerant performance of the SICH-3 among various SICH samples.

The hydrogel sample of PAA-r-BVIT was brittle and failed to perform the cyclic test. The hydrogel sample of PAA/PEO showed a plastic deformation of 6% and 17.3%, respectively, in the 1st and 100th cycle (Fig. S6a), and its maximum stress and Young's modulus remained above 80% after 100 compressive cycles (Fig. S6b). A soft but weak network was observed within the PAA/PEO, and the energy loss coefficient of PAA/PEO was 0.48, which was much larger than those of SICH samples. The SICH-1 sample exhibited a small plastic deformation of 5.4% (Fig. S7a), and its maximum stress and Young's modulus remained above 62% after 500 cycles (Fig. S7b). The SICH-2 sample exhibited a small plastic deformation of 3% (Fig. S8a) with the maximum stress and

Young's modulus remaining above 62% after 1000 cycles (Fig. S8b). Although no plastic deformation occurred, the mechanical properties of the SICH-4 were relatively poor, and the maximum stress and Young's modulus remained above 75% after 1000 cycles (Figs. S9a, S9b) By contrast, the SICH-3 sample remained a high recovery of mechanical strength and stiffness with no obvious plastic deformation.

The ionic conductivities of SICH samples were measured using the electrical impedance spectroscopy (EIS) method. The EIS curves of all the samples are composed of a small semicircle and a straight line (Fig. 4a). The starting point of the semicircle is defined as the electrolyte resistance and the diameter of the semicircle is defined as the charge transfer resistance.[54–57] The charge transfer resistances of SICH samples generally increased with the raising AA/BVIT molar ratio, and their ionic conductivities were in the order of 10^{-2} S m^{-1} (Fig. 4b). The ionic conductivity of SICH-3 reached as high as 0.036 S m^{-1}, similar to other ionic conductors in the literature.[19,58,59] Fig. 4c and 4d show the relative resistance variations of the SICH-3 under the stretching/releasing and compressing/releasing processes, demonstrating that its ionic conductivity is sensitive to the variations of the applied strains and pressures. Additionally, the SICH was connected to a complete circuit to light a bulb. The brightness of the bulb became dim during the stretching (Fig. 4e, Movie S3) but bright during the compressing (Fig. 4f, Movie S4). This phenomenon further indicates that the ionic conductivity of the SICH is sensitive to variations of strain and pressure.

As summarized in Table 1, tensile mechanical properties of the SICH-3 kept above 89% after 400 stretching-releasing cycles, and its compressive mechanical properties kept above 74% after 2000 compressing-releasing cycles, demonstrating its excellent fatigue resistance. The ionic conductivity of the SICH-3 was comparable to most of the PIL-based hydrogels in the literature (Table 1). With the integration of high stretchability/compressibility, excellent fatigue resistance and high ionic conductivity, the SICH-3 can serve as a highly stretchable and compressible ionic conductor for both capacitive and resistive ionic sensors. When the SICH-3 worked as a capacitive pressure sensor, the

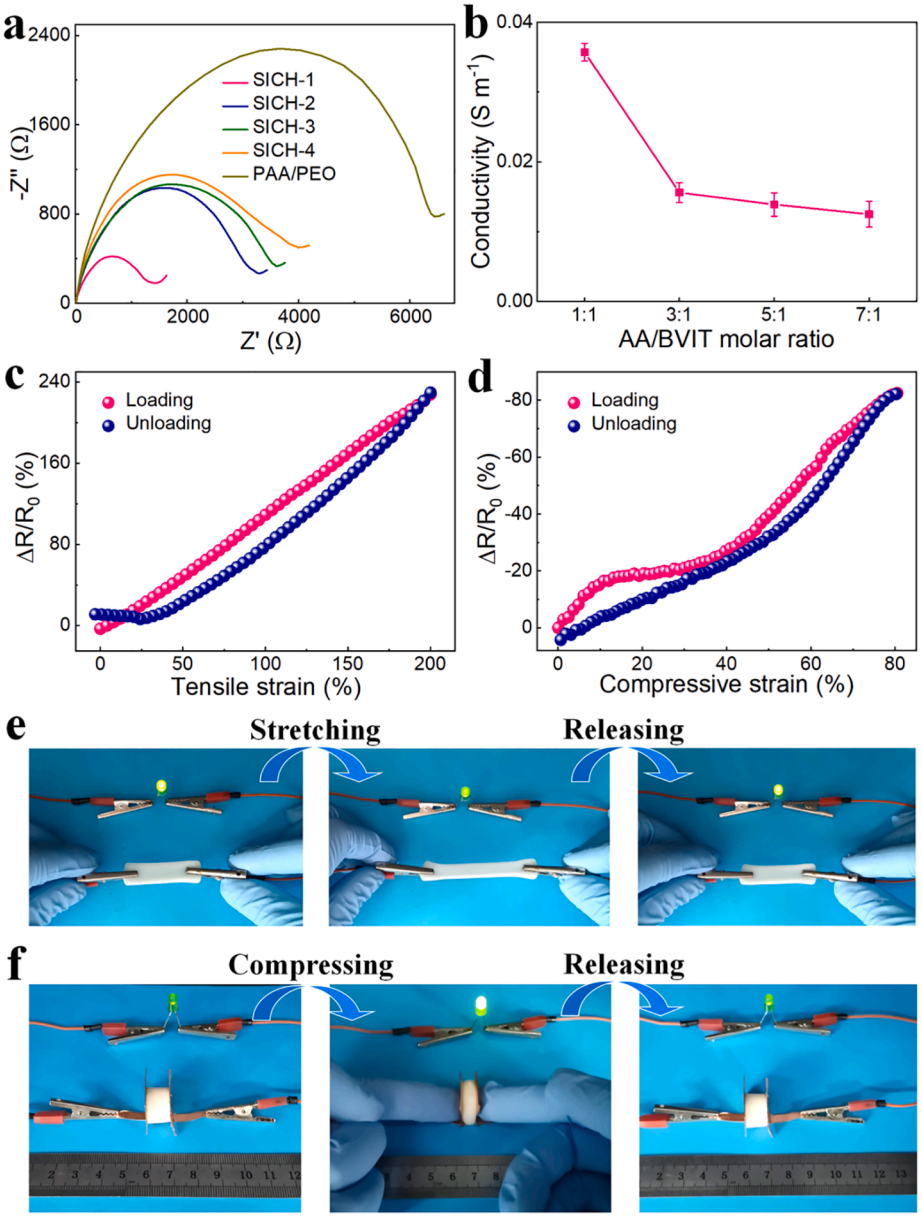

Fig. 4. Ionic conductivities of the SICH under complex deformations. (a) EIS curves of hydrogel samples of SICH and PAA/PEO. (b) Calculated ionic conductivities of the SICH. Relative resistance variation of the SICH under (c) stretching and (d) compressing. Photographs showing the brightness of a LED lamp changing when SICH is subjected to (e) stretching and (f) compressing in a circuit.

Table 1
Summary of mechanical properties, ionic conductivities and sensing performances of PIL hydrogel-based sensors.

Samples	Tensile strength (kPa)/ Strain (%)	Compressive strength (kPa)/ Strain (%)	Tensile cycles/ Recovery	Compressive cycles/ Recovery	Ionic conductivity (S m^{-1})	Sensing type	Work range	Gauge factor	Sensitivity (kPa^{-1})	Ref.
PIL hydrogel (10% KCl)	260/710	–	–	–	0.8	Capacitance/ Resistance/ Triboelectricity	1.1–45 kPa 0–160%	0.027 (80–160%)	0.0057	[5]
PHEMA/ PSBMA/ Laponite	270/2000	–	–	–	0.099	Resistance	0–100%	1.8 (30–100%)	–	[11]
PAA-co-DMAPS	2000/ 10000	50/50	–	–	0.002	Capacitance/ Resistance	0–100%	–	–	[63]
PMAA-co-DMAPS	300/2500	–	50/78%	–	–	Capacitance/ Resistance	0–5 kPa 0–100%	1 (0–100%)	0.09	[64]
P(AAm/ AMPS)-AFPS	50/1500	0.07/85	10/-	10/-	1.7	Resistance	0–900%	1.58 (0–100%) 4.82 (100–500%) 8.99 (500–900%)	–	[65]
PDA-clay-PSBMA	77/1000	4200/85	5/58.5%	–	0.02	Resistance	0–670%	1.25 (0–80%) 2 (0–200%)	–	[66]
PVA/ PSBMA	228/400	6500/95	–	–	0.0429	Resistance	0–300%	0.8 (0–50%) 1.5 (50–300%)	–	[67]
SICH-3	39/321	630/85	400/89%	2000/74%	0.036	Capacitance/ Resistance	0–8 kPa 0–300%	1.1 (0–300%)	0.22 (0–1.4), 0.13 (1.4–4.7), 0.07 (4.7–8)	This work

pressure applied to the sensor was measured by detecting the changes of capacitance ($\Delta C/C_0$), which was related to the area (A) of the ionic conductor and thickness (d) of the dielectric layer, according to the capacitance formula. The relationship between $\Delta C/C_0$ and the pressure applied to the sensor was investigated (Fig. 5a) and quantified by the sensitivity (S) value which was defined as the $\delta(\Delta C/C_0)/\delta P$.[2,60] Similar to previously reported pressure sensors based on ionic hydrogels, the sensitivity of the SICH capacitive pressure sensor varied with the pressure, and the curve can be divided into multiple regions. [16,25,53,61] The sensitivity was 0.22, 0.13 and 0.07 kPa^{-1}, when the loading pressure was in the range of 0–1.4, 1.4–4.7 and 4.7–8 kPa, respectively. The explanation of the relatively small sensitivity at the high pressure is that excessive deformations of hydrogels might result in the limitation of ionic shuttle distance.[62] The capacitive pressure sensor could perceive diverse dynamic pressures and real-time produce stable capacitive variations (Fig. S10a). Additionally, the capacitive response of the ionic sensor kept consistent with its mechanical behavior. The capacitive pressure sensor was applied to a constant pressure of 4 kPa at various loading speeds of 5–20 mm min^{-1} (Fig. 5b). The constant capacitive variation demonstrated that the ionic sensor

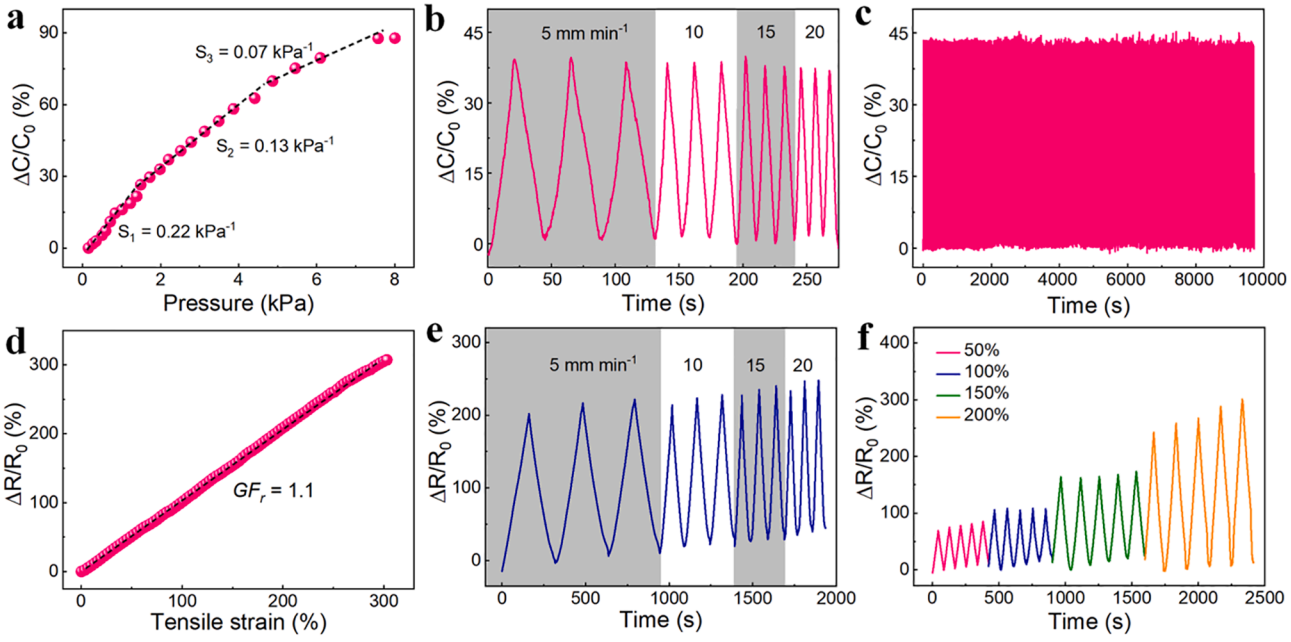

Fig. 5. Capacitive/resistive sensing performance of the bimodal ionic sensor based on SICH. (a) Relative capacitance variation as a function of applied pressure. (b) Relative capacitance variation at a constant pressure of 4 kPa with various applied speeds. (c) 500 loading–unloading compressive cyclic tests under the pressure of 4 kPa. (d) Relative resistance variation as a function of tensile strain. (e) Relative resistance variation at a constant strain of 200% with various applied speeds. (f) Relative resistance variation with various tensile strains.

possessed the potential in detecting dynamic pressures. The response time of the capacitive pressure sensor was not accurately measured since the value is lower than the limitation of the measurement instrument (Fig. S10b). In addition to the sensitivity and response time, the fatigue resistance was also a crucial performance for a pressure sensor. Therefore, 500 loading/unloading compressive cycles at a constant pressure of 4 kPa were applied to the SICH-3 capacitive pressure sensor (Fig. 5c). Stable and repeatable capacitive variations were observed throughout the cycles, revealing the high stability and good reliability of the capacitive pressure sensor. In addition to pressure, the capacitive ionic sensor is capable of monitoring dynamic strains. For example, the capacitive sensor produced a large capacitive response to the strain, suggesting its high sensitivity to the strain (Fig. S11a). A good linear relationship between the $\Delta C/C_0$ and strain was observed in the strain range of 0–100%. Gauge factor (*GF*) was generally considered as a vital performance to evaluate the sensitivity of a strain sensor. It was defined as the $\delta(\Delta C/C_0)/\delta\varepsilon$ and the present sensor was calculated as 1.1. The durability test of the stretchable sensing performance over 5 cycles demonstrated excellent stability of the capacitive strain sensor (Fig. S11b). In short, the capacitive sensor based on the SICH-3 had a high sensitivity to the pressure, good linear response to the strain and high fatigue resistance stability for practical uses.

Subsequently, the stretchable and compressive sensing performance of the SICH-3 in a resistive mode was also characterized. Surprisingly, the relative resistance change ($\Delta R/R_0$) and strain always kept a good linear relationship in the strain range of 0–300% (Fig. 5d). Gauge factor (GF_r) was defined as the $\delta(\Delta R/R_0)/\delta\varepsilon$ to evaluate the sensitivity of the resistive strain sensor, and the current sensor was calculated as 1.1. The strain sensing performance was measured at various loading speeds of 5–20 mm min^{-1} (Fig. 5e). The relative resistances showed no vibrations with the various loading speeds, revealing the resistive sensor can steadily detect the strain. Moreover, the resistive sensor is capable of perceiving various strains of 50%, 100%, 150% and 200%, and producing steady and repeatable responses (Fig. 5f). Cyclic loading/unloading sensing performance tests were measured to evaluate the fatigue resistance of the resistive strain sensor (Fig. S12a). After 100 cycles under a strain of 200%, the relative resistive variation drifted upwards due to the water loss of hydrogel samples and inevitable deformation hysteresis. The resistive strain sensor showed a fast response time and recovery time within 80 and 90 ms (Fig. S12b), respectively. This slight signal lag was related to the inherent viscoelasticity of hydrogels.[62] In addition to the strain, the resistive sensor could also monitor the dynamic pressures. Fig. S13a showed the $\Delta R/R_0$ as a function of the applied pressure to the sensor. The sensitivity was defined as $\delta(\Delta R/R_0)/\delta P$, and the present device was calculated as 0.17, 0.02 and 0.01 kPa^{-1}, corresponding to the applied pressure ranging among 0–1, 1–18, 18–34 kPa, respectively. Continuous 100 loading/unloading tests at a constant pressure of 34 kPa were performed to evaluate the fatigue resistance of the sensor (Fig. S13b). The relative resistive variation decreased ~14% at the first 300 s, but drifted slightly upward at later periods, indicating great durability of the resistive sensor. Table 1 showed the comparisons of the sensing performances of our SICH with PIL-based hydrogels in the literature. The gauge factor of the SICH sensor was kept at ~1.1 in a wide strain range of 0–300% and the sensitivity was comparable to other reported values. Therefore, the resistive sensor based on SICH showed a good linear response to the strain, a wide range of pressure detection and a rapid response time.

As a demonstration, the SICH can serve as a bimodal ionic sensor for human-motion detection. The SICH was attached to various parts of the human body and the relative capacitive and resistive variations were recorded in real-time. The movements of the finger and the elbow bending to different angles of 30°, 60° and 90° were monitored (Fig. 6a, b). The relative capacitance variations always corresponded with the different bending angles and these processes could be repeated. Furthermore, when the finger or elbow is held at a certain bending angle, the relative capacitance variation also kept the value steadily. The bimodal ionic sensor was also utilized to monitor physiological activities in a resistive operating mode. Fig. 6c exhibited the real-time resistance variation when the ionic skin adhered to the throat of a volunteer. The slight changes caused by test words such as “hi” and “hello” can be detected by the resistive sensor quickly and accurately. The movement of the knee was also able to be monitored by the sensor (Fig. 6d). As the

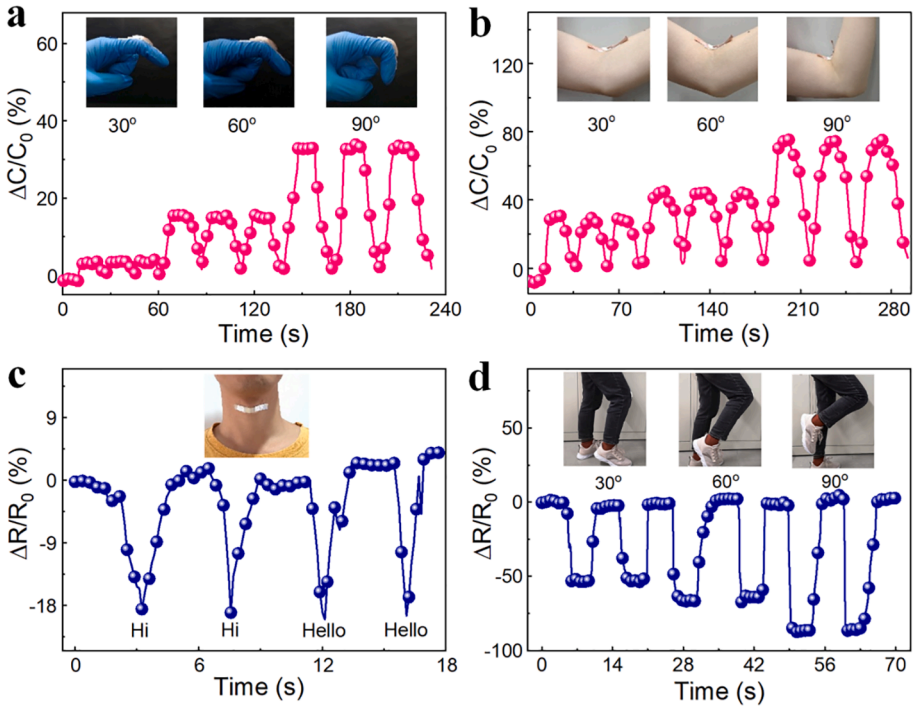

Fig. 6. Wearable sensing performance of the bimodal ionic skin sensor based on SICH. Relative capacitance variations in response to (a) finger and (b) elbow bending, and relative resistance variations in response to (c) speaking and (d) knee bending.

bending angle increased from 0° to 90°, the relative resistance variation gradually increased and could be held steadily when the bending angle was maintained.

4. Conclusions

In summary, the SICH with a semi-interpenetrating network was fabricated by a hydrogel-network constrained polymerization strategy, during which the covalent chemical bond cross-linked random copolymer (PAA-r-BVIT) network was in-situ formed in the PEO network. Intermolecular hydrogen-bonded interaction between the PAA-r-BVIT and PEO as well as intramolecular electrostatic interaction among the PAA-r-BVIT were synchronously achieved. As a result, the as-obtained SICH is capable of being shaped and cut into various shapes, stretched up to ~300%, compressed to ~85%, and recovered immediately upon the external force released. Due to its high mechanical robustness, excellent fatigue resistance and good ionic conductivity, the SICH can readily work as a highly deformation-tolerant ionic conductor for a capacitive/resistive bimodal ionic sensor. The capacitive-type SICH ionic sensor exhibited a wide response range to dynamic pressures (0–8 kPa) and high fatigue resistance over 500 cycles. The resistive-type SICH ionic sensor had high linearity over the strain range of 0–300% and showed in real-time resistance response within 80 ms. The wearable SICH ionic sensor was assembled, achieving real-time monitoring of complex human motions of speaking and various joint bending. This work provides an exploration for developing ionic conductive hydrogels with high mechanical strength and excellent fatigue resilience and their applications in bimodal ionic sensors with high sensitivity, linearity, wide detecting range and durability.

Declaration of Competing Interest

The authors declare that they have no known competing financial interests or personal relationships that could have appeared to influence the work reported in this paper.

Acknowledgments

This work was supported by the National Natural Science Foundation of China (21875033), the Fundamental Research Funds for the Central Universities (2232020G-02), the Shanghai Rising-Star Program (18QA1400200), the Shanghai Scientific and Technological Innovation Project (18JC1410600), and Ministry of Education of the People's Republic of China (6141A02033233).

Appendix A. Supplementary data

Supplementary data to this article can be found online at https://doi.org/10.1016/j.cej.2021.128506.

References

[1] H.R. Lee, C.C. Kim, J.Y. Sun, Stretchable ionics - a promising candidate for upcoming wearable devices, Adv. Mater. 30 (2018) 1704403.
[2] Z. Wang, Y. Cong, J. Fu, Stretchable and tough conductive hydrogels for flexible pressure and strain sensors, J. Mater. Chem. B 8 (16) (2020) 3437–3459, https://doi.org/10.1039/C9TB02570G.
[3] T.X. Zhu, Y. Cheng, C.Y. Cao, J.J. Mao, L.Q. Li, J.Y. Huang, S.W. Gao, X.L. Dong, Z. Chen, Y.K. Lai, A semi-interpenetrating network ionic hydrogel for strain sensing with high sensitivity, large strain range, and stable cycle performance, Chem. Eng. J. 385 (2020), 123912.
[4] M.L. Hammock, A. Chortos, B.C. Tee, J.B. Tok, Z. Bao, 25th anniversary article: The evolution of electronic skin (e-skin): a brief history, design considerations, and recent progress, Adv. Mater. 25 (2013) 5997–6038.
[5] Z. Liu, Y. Wang, Y. Ren, G. Jin, C. Zhang, W. Chen, F. Yan, Poly(ionic liquid) hydrogel-based anti-freezing ionic skin for a soft robotic gripper, Mater. Horiz. 7 (3) (2020) 919–927, https://doi.org/10.1039/C9MH01688K.
[6] Y. Guo, M. Zhong, Z. Fang, P. Wan, G. Yu, A Wearable Transient Pressure Sensor Made with MXene Nanosheets for Sensitive Broad-Range Human–Machine Interfacing, Nano Lett. 19 (2) (2019) 1143–1150, https://doi.org/10.1021/acs.nanolett.8b04514.s001.
[7] P. Cai, B. Hu, W.R. Leow, X. Wang, X.J. Loh, Y.L. Wu, X. Chen, Biomechano-interactive materials and interfaces, Adv. Mater. 30 (2018) 1800572.
[8] C. Yang, Z. Suo, Hydrogel ionotronics, Nat. Rev. Mater. 3 (6) (2018) 125–142, https://doi.org/10.1038/s41578-018-0018-7.
[9] J.-Y. Sun, C. Keplinger, G.M. Whitesides, Z. Suo, Ionic skin, Adv. Mater. 26 (45) (2014) 7608–7614, https://doi.org/10.1002/adma.201403441.
[10] J.S. Kim, S.C. Lee, J. Hwang, E. Lee, K. Cho, S.J. Kim, D.H. Kim, W.H. Lee, Enhanced sensitivity of iontronic graphene tactile sensors facilitated by spreading of ionic liquid pinned on graphene grid, Adv. Funct. Mater. 30 (2020) 1908993.
[11] L. Wang, G. Gao, Y. Zhou, T. Xu, J. Chen, R. Wang, R. Zhang, J. Fu, Tough, Adhesive, Self-Healable, and Transparent Ionically Conductive Zwitterionic Nanocomposite Hydrogels as Skin Strain Sensors, ACS Appl. Mater. Interfaces 11 (3) (2019) 3506–3515, https://doi.org/10.1021/acsami.8b20755.s003.
[12] J. Mao, C. Zhao, Y. Li, D. Xiang, Z. Wang, Highly stretchable, self-healing, and strain-sensitive based on double-crosslinked nanocomposite hydrogel, Compos. Commun. 17 (2020) 22–27, https://doi.org/10.1016/j.coco.2019.10.007.
[13] Z. Lei, Q. Wang, S. Sun, W. Zhu, P. Wu, A bioinspired mineral hydrogel as a self-healable, mechanically adaptable ionic skin for highly sensitive pressure sensing, Adv. Mater. 29 (2017) 1700321.
[14] Q. Liu, Z. Liu, C. Li, K. Xie, P. Zhu, B. Shao, J. Zhang, J. Yang, J. Zhang, Q. Wang, C. F. Guo, Highly transparent and flexible iontronic pressure sensors based on an opaque to transparent transition, Adv. Sci. 7 (2020) 2000348.
[15] Z.G. Qiu, Y.B. Wan, W.H. Zhou, J.Y. Yang, J.L. Yang, J. Huang, J.M. Zhang, Q. X. Liu, S.Y. Huang, N.N. Bai, Z.G. Wu, W. Hong, H. Wang, C.F. Guo, Ionic skin with biomimetic dielectric layer templated from calathea zebrine leaf, Adv. Funct. Mater. 28 (2018) 1802343.
[16] V. Amoli, J.S. Kim, E. Jee, Y.S. Chung, S.Y. Kim, J. Koo, H. Choi, Y. Kim, D.H. Kim, A bioinspired hydrogen bond-triggered ultrasensitive ionic mechanoreceptor skin, Nat. Commun. 10 (2019) 4019.
[17] Y. Cao, T.G. Morrissey, E. Acome, S.I. Allec, B.M. Wong, C. Keplinger, C. Wang, A transparent, self-healing, highly stretchable ionic conductor, Adv. Mater. 29 (2017) 1605099.
[18] H.L. Sun, K.K. Zhou, Y.F. Yu, X.Y. Yue, K. Dai, G.Q. Zheng, C.T. Liu, C.Y. Shen, Highly stretchable, transparent, and bio-friendly strain sensor based on self-recovery ionic-covalent hydrogels for human motion monitoring, Macromol. Mater. Eng. 304 (2019) 1900227.
[19] Z. Cao, H. Liu, L. Jiang, Transparent, mechanically robust, and ultrastable ionogels enabled by hydrogen bonding between elastomers and ionic liquids, Mater. Horiz. 7 (3) (2020) 912–918, https://doi.org/10.1039/C9MH01699F.
[20] B. Yang, W. Yuan, Highly Stretchable, Adhesive, and Mechanical Zwitterionic Nanocomposite Hydrogel Biomimetic Skin, ACS Appl. Mater. Interfaces 11 (43) (2019) 40620–40628, https://doi.org/10.1021/acsami.9b14040.s001.
[21] M.H. Liao, P.B. Wan, J.R. Wen, M. Gong, X.X. Wu, Y.G. Wang, R. Shi, L.Q. Zhang, Wearable, healable, and adhesive epidermal sensors assembled from mussel-inspired conductive hybrid hydrogel framework, Adv. Funct. Mater. 27 (2017) 1703852.
[22] H. Liao, X.L. Guo, P.B. Wan, G.H. Yu, Conductive mxene nanocomposite organohydrogel for flexible, healable, low-temperature tolerant strain sensors, Adv. Funct. Mater. 29 (2019) 1904507.
[23] C. Ma, Y. Wang, Z. Jiang, Z. Cao, H. Yu, G. Huang, Q. Wu, F. Ling, Z. Zhuang, H. Wang, J. Zheng, J. Wu, Wide-range linear viscoelastic hydrogels with high mechanical properties and their applications in quantifiable stress-strain sensors, Chem. Eng. J. 399 (2020), 125697.
[24] C. Keplinger, J.-Y. Sun, C.C. Foo, P. Rothemund, G.M. Whitesides, Z. Suo, Stretchable, transparent, ionic conductors, Science 341 (6149) (2013) 984–987, https://doi.org/10.1126/science:1240228.
[25] H. Liu, X. Wang, Y. Cao, Y. Yang, Y. Yang, Y. Gao, Z. Ma, J. Wang, W. Wang, D. Wu, Freezing-tolerant, highly sensitive strain and pressure sensors assembled from ionic conductive hydrogels with dynamic cross-links, ACS Appl. Mater. Interfaces 12 (22) (2020) 25334–25344, https://doi.org/10.1021/acsami.0c06067.s005.
[26] N. Bai, L. Wang, Q. Wang, J. Deng, Y. Wang, P. Lu, J. Huang, G. Li, Y. Zhang, J. Yang, K. Xie, X. Zhao, C.F. Guo, Graded intrafillable architecture-based iontronic pressure sensor with ultra-broad-range high sensitivity, Nat. Commun. 11 (2020) 209.
[27] H. Zhang, W. Niu, S. Zhang, Extremely stretchable, sticky and conductive double-network ionic hydrogel for ultra-stretchable and compressible supercapacitors, Chem. Eng. J. 387 (2020), 124105.
[28] S.-H. Shin, W. Lee, S.-M. Kim, M. Lee, J.M. Koo, S.Y. Hwang, D.X. Oh, J. Park, Ion-conductive self-healing hydrogels based on an interpenetrating polymer network for a multimodal sensor, Chem. Eng. J. 371 (2019) 452–460, https://doi.org/10.1016/j.cej.2019.04.077.
[29] S. Xia, S. Song, G. Gao, Robust and flexible strain sensors based on dual physically cross-linked double network hydrogels for monitoring human-motion, Chem. Eng. J. 354 (2018) 817–824, https://doi.org/10.1016/j.cej.2018.08.053.
[30] X.-H. Wang, F. Song, D. Qian, Y.-D. He, W.-C. Nie, X.-L. Wang, Y.-Z. Wang, Strong and tough fully physically crosslinked double network hydrogels with tunable mechanics and high self-healing performance, Chem. Eng. J. 349 (2018) 588–594, https://doi.org/10.1016/j.cej.2018.05.081.
[31] Z. Guo, H. Gu, Y. He, Y. Zhang, W. Xu, J. Zhang, Y. Liu, L. Xiong, A. Chen, Y. Feng, Dual dynamic bonds enable biocompatible and tough hydrogels with fast self-recoverable, self-healable and injectable properties, Chem. Eng. J. 388 (2020), 124282.
[32] M.A. Darabi, A. Khosrozadeh, R. Mbeleck, Y. Liu, Q. Chang, J. Jiang, J. Cai, Q. Wang, G. Luo, M. Xing, Skin-inspired multifunctional autonomic-intrinsic

conductive self-healing hydrogels with pressure sensitivity, stretchability, and 3d printability, Adv. Mater. 29 (2017) 1700533.
[33] Y. Wang, M. Tebyetekerwa, Y. Liu, M. Wang, J. Zhu, J. Xu, C. Zhang, T. Liu, Extremely stretchable and healable ionic conductive hydrogels fabricated by surface competitive coordination for human-motion detection, Chem. Eng. J. (2020) 127637, https://doi.org/10.1016/j.cej.2020.127637.
[34] M.X. Wang, Y.M. Chen, Y. Gao, C. Hu, J. Hu, L.i. Tan, Z. Yang, Rapid self-recoverable hydrogels with high toughness and excellent conductivity, ACS Appl. Mater. Interfaces 10 (31) (2018) 26610–26617, https://doi.org/10.1021/acsami.8b06567.s002.
[35] R. Bai, J. Yang, Z. Suo, Fatigue of hydrogels, Eur. J. Mech. A. Solids 74 (2019) 337–370, https://doi.org/10.1016/j.euromechsol.2018.12.001.
[36] H.J. Zhang, T.L. Sun, A.K. Zhang, Y. Ikura, T. Nakajima, T. Nonoyama, T. Kurokawa, O. Ito, H. Ishitobi, J.P. Gong, Tough physical double-network hydrogels based on Amphiphilic triblock copolymers, Adv. Mater. 28 (24) (2016) 4884–4890, https://doi.org/10.1002/adma.201600466.
[37] T.R. Rooney, R.A. Hutchinson, Monomer structure and solvent effects on copolymer composition in (meth)acrylate radical copolymerization, Ind. Eng. Chem. Res. 57 (15) (2018) 5215–5227, https://doi.org/10.1021/acs.iecr.8b00451.
[38] W. Qian, J. Texter, F. Yan, Frontiers in poly(ionic liquid)s: syntheses and applications, Chem. Soc. Rev. 46 (2017) 1124–1159.
[39] F. Lai, C. Yang, R. Lian, K. Chu, J. Qin, W. Zong, D. Rao, J. Hofkens, X. Lu, T. Liu, Three-phase boundary in cross-coupled micro-mesoporous networks enabling 3d-printed and ionogel-based quasi-solid-state micro-supercapacitors, Adv. Mater. 32 (2020) 2002474.
[40] Y.-S. Ye, J. Rick, B.-J. Hwang, Ionic liquid polymer electrolytes, J. Mater. Chem. A 1 (8) (2013) 2719–2743, https://doi.org/10.1039/C2TA00126H.
[41] N.M. Vaghela, N.V. Sastry, V.K. Aswal, Surface active and aggregation behavior of methylimidazolium-based ionic liquids of type [C n mim] [X], n = 4, 6, 8 and [X] = Cl−, Br−, and I− in water, Colloid Polym. Sci. 289 (3) (2011) 309–322, https://doi.org/10.1007/s00396-010-2332-5.
[42] Y.S. Ye, Y.A. Elabd, Anion exchanged polymerized ionic liquids: High free volume single ion conductors, Polymer 52 (2011) 1309–1317.
[43] X.N. Zhang, Y.J. Wang, S. Sun, L. Hou, P. Wu, Z.L. Wu, Q. Zheng, A Tough and Stiff Hydrogel with Tunable Water Content and Mechanical Properties Based on the Synergistic Effect of Hydrogen Bonding and Hydrophobic Interaction, Macromolecules 51 (20) (2018) 8136–8146, https://doi.org/10.1021/acs.macromol.8b01496.s001.
[44] Z. Lv, J.-N. Qiao, Y.-N. Song, X.u. Ji, J.-H. Tang, D.-X. Yan, J. Lei, Z.-M. Li, Baroplastics with Robust Mechanical Properties and Reserved Processability through Hydrogen-Bonded Interactions, ACS Appl. Mater. Interfaces 11 (12) (2019) 12008–12016, https://doi.org/10.1021/acsami.8b20676.s001.
[45] Z. Zhang, Z. Gao, Y. Wang, L. Guo, C. Yin, X. Zhang, J. Hao, G. Zhang, L. Chen, Eco-Friendly, Self-Healing Hydrogels for Adhesive and Elastic Strain Sensors, Circuit Repairing, and Flexible Electronic Devices, Macromolecules 52 (6) (2019) 2531–2541, https://doi.org/10.1021/acs.macromol.8b02466.s001.
[46] Q. Zhao, M. Yin, A.P. Zhang, S. Prescher, M. Antonietti, J. Yuan, Hierarchically structured nanoporous poly(ionic liquid) membranes: Facile preparation and application in fiber-optic ph sensing, J. Am. Chem. Soc. 135 (2013) 5549–5552.
[47] Q. Zhu, Y. Li, W. Wang, G. Sun, K. Yan, D. Wang, High performance HKUST-1@PVA-co-PE/PVA hybrid hydrogel with enhanced selective adsorption, Compos. Commun. 10 (2018) 36–40, https://doi.org/10.1016/j.coco.2018.05.005.
[48] G.S. Song, Z.Y. Zhao, X. Peng, C.C. He, R.A. Weiss, H.L. Wang, Rheological behavior of tough pvp-in situ-paam hydrogels physically cross-linked by cooperative hydrogen bonding, Macromolecules 49 (2016) 8265-8273.
[49] H. Guo, J. Zhou, Q. Li, Y. Li, W. Zong, J. Zhu, J. Xu, C. Zhang, T.X. Liu, Emerging dual-channel transition-metal-oxide quasiaerogels by self-embedded templating, Adv. Funct. Mater. 30 (2020) 2000024.
[50] H. Guo, Q. Feng, K. Xu, J. Xu, J. Zhu, C. Zhang, T.X. Liu, Self-templated conversion of metallogel into heterostructured tmp@carbon quasiaerogels boosting bifunctional electrocatalysis, Adv. Funct. Mater. 29 (2019) 1903660.
[51] Z.T. Zhao, A.R. Mao, W.W. Gao, H. Bai, A facile in situ method to fabricate transparent, flexible polyvinyl alcohol/zno film for uv-shielding, Compos. Commun. 10 (2018) 157–162.
[52] X. Li, H. Wang, D. Li, S. Long, G. Zhang, Z. Wu, Dual ionically cross-linked double-network hydrogels with high strength, toughness, swelling resistance, and improved 3d printing processability, ACS Appl. Mater. Interfaces 10 (2018) 31198–31207.
[53] S. Xia, Q. Zhang, S. Song, L. Duan, G. Gao, Bioinspired dynamic cross-linking hydrogel sensors with skin-like strain and pressure sensing behaviors, Chem. Mater. 31 (2019) 9522–9531.
[54] L. Li, Y. Zhang, H. Lu, Y. Wang, J. Xu, J. Zhu, C. Zhang, T. Liu, Cryopolymerization enables anisotropic polyaniline hybrid hydrogels with superelasticity and highly deformation-tolerant electrochemical energy storage, Nat. Commun. 11 (2020) 62.
[55] T. Zhu, S. Liu, K. Wan, C. Zhang, Y. Feng, W. Feng, T. Liu, Fluorine and nitrogen dual-doped porous carbon nanosheet-enabled compact electrode structure for high volumetric energy storage, ACS Appl. Energy Mater. 3 (2020) 4949–4957.
[56] Y. Zheng, H. Song, S. Chen, X. Yu, J. Zhu, J. Xu, K.A.I. Zhang, C. Zhang, T. Liu, Metal-free multi-heteroatom-doped carbon bifunctional electrocatalysts derived from a covalent triazine polymer, Small 16 (2020) 2004342.
[57] Y. Wang, K. Wang, C. Zhang, J. Zhu, J. Xu, T. Liu, Solvent-exchange strategy toward aqueous dispersible mos2 nanosheets and their nitrogen-rich carbon sphere nanocomposites for efficient lithium/sodium ion storage, Small 15 (2019) 1903816.
[58] Z. Lei, P. Wu, A highly transparent and ultra-stretchable conductor with stable conductivity during large deformation, Nat. Commun. 10 (2019) 3429.
[59] L. Shi, T. Zhu, G. Gao, X. Zhang, W. Wei, W. Liu, S. Ding, Highly stretchable and transparent ionic conducting elastomers, Nat. Commun. 9 (2018) 2630.
[60] M.Z. Tang, R. Zhang, J. Fang, S.Q. Li, Y.X. Xu, G.S. Huang, Ductile composites with strain hardening behavior constructing highly sensitive electronic sensor, Compos. Commun. 15 (2019) 20–24.
[61] S.H. Li, H.Y. Pan, Y.T. Wang, J.Q. Sun, Polyelectrolyte complex-based self-healing, fatigue-resistant and anti-freezing hydrogels as highly sensitive ionic skins, J. Mater. Chem. A 8 (2020) 3667–3675.
[62] G. Ge, Y.Z. Zhang, J.J. Shao, W.J. Wang, W.L. Si, W. Huang, X.C. Dong, Stretchable, transparent, and self-patterned hydrogel-based pressure sensor for human motions detection, Adv. Funct. Mater. 28 (2018) 1802576.
[63] Z. Lei, P. Wu, A supramolecular biomimetic skin combining a wide spectrum of mechanical properties and multiple sensory capabilities, Nat. Commun. 9 (2018) 1134.
[64] Z. Lei, P. Wu, Zwitterionic skins with a wide scope of customizable functionalities, ACS Nano 12 (2018) 12860–12868.
[65] J.J. Xu, R.N. Jing, X.Y. Ren, G.H. Gao, Fish-inspired anti-icing hydrogel sensors with low-temperature adhesion and toughness, J. Mater. Chem. A 8 (2020) 9373–9381.
[66] X.J. Pei, H. Zhang, Y. Zhou, L.J. Zhou, J. Fu, Stretchable, self-healing and tissue-adhesive zwitterionic hydrogels as strain sensors for wireless monitoring of organ motions, Mater. Horiz. 7 (2020) 1872–1882.
[67] Z. Wang, J. Chen, L. Wang, G. Gao, Y. Zhou, R. Wang, T. Xu, J. Yin, J. Fu, Flexible and wearable strain sensors based on tough and self-adhesive ion conducting hydrogels, J. Mater. Chem. B 7 (2019) 24–29.